JOURNAL OF PROPULSION AND POWER
Vol. 10, No. 2, March–April 1994

# Prediction of NOx Production in a Turbulent Hydrogen-Air Jet Flame

Suresh Menon*
*Georgia Institute of Technology, Atlanta, Georgia 30332*
Patrick A. McMurtry†
*University of Utah, Salt Lake City, Utah 84112*
Alan R. Kerstein‡
*Sandia National Laboratories, Livermore, California 94550*
and
J.-Y. Chen§
*University of California, Berkeley, Berkeley, California 94720*

**A major concern in the numerical study of turbulent nonpremixed flames is the accurate prediction of trace species. The production of pollutants such as NOx during unsteady combustion needs to be understood and predicted accurately so that the design of the next generation's combustion systems can meet the forthcoming stricter environmental restrictions. Numerical studies using steady-state methods cannot account for the unsteady phenomena in the mixing region, and therefore, fail to accurately predict the NOx production that could occur. A novel unsteady mixing model is demonstrated here that accounts for all the length scales associated with mixing and molecular diffusion processes. Finite-rate kinetics in the form of a reduced mechanism have been used to study hydrogen-air nonpremixed jet flames. NOx production in these jet flames was also predicted. Comparisons with experimental data and pdf calculations show good agreement, thereby, providing validation of the mixing model.**

## I. Introduction

TO develop the next generation of high-speed civil transport (HSCT) aircraft, a significant reduction in pollutant emissions from the engine must first be demonstrated. Emissions that must be reduced include, NOx emissions into the stratosphere during supersonic flight, and the NOx, CO, and unburned hydrocarbons emissions near urban areas during idling and takeoff/landing operations. Extensive investigations have been carried out by various researchers[1,2] to identify and evaluate various advanced combustor designs that could result in reduced pollutant emissions. Various low-NOx combustor concepts—i.e., lean-premixed-prevaporized (LPP), rich burn/quick quench/lean burn (RQL), and direct injection (DI) are being studied,[2] and their NOx emission characteristics have been determined over a wide range of inlet temperatures, fuel-air ratios, and pressures.

For aircraft such as the HSCT, which will have a wide range of operating conditions, the RQL combustor configuration has good potential for significantly reducing NOx emissions. In such a configuration, the primary combustion occurs in a fuel-rich environment. Downstream, air is injected to rapidly dilute the fuel-rich mixture exiting from the primary stage so that a uniformly mixed fuel-lean mixture burns in the secondary stage. This concept, although more complex than the LPP and the DI concepts, attempts to minimize (if not completely inhibit) NOx formation in the hot primary stage by limiting or eliminating free oxygen atoms, and in the fuel-lean secondary stage by reducing the combustion temperature. NOx will form in regions where the secondary air mixes with the hot fuel-rich mixture exiting from the primary zone (in the quench region), especially in regions where the fuel-air ratio becomes locally close to stoichiometric. However, the exact mechanism of NOx production in the highly unsteady mixing zone has not yet been clarified. The RQL concept has good stability characteristics due to its fuel-rich zone and can be used with current jet fuels, as well as, alternative fuels containing large amounts of fuel-bound nitrogen.[2] Thus, if an effective (low NOx producing) technique to rapidly mix the secondary air with the fuel-rich primary mixture can be determined, then this concept may become practically feasible.

At present, there is an extensive experimental program underway to evaluate low-NOx combustors such as the LPP and the RQL.[3] Detailed measurements inside and immediately downstream of the quench zone will be required to determine the efficiency of the rapid mixing concepts. Experimentally studying various types of rapid mixing concepts such as swirl jets and jets in crossflow can be expensive, and unless the characteristic length and time scales involved in these unsteady mixing concepts are determined and their relevance to NOx production quantified, experiments alone may not provide the necessary guidelines to build production engines. Typically, numerical prediction methods are used to complement experimental studies, both to understand the dynamics and to extend the experimental results to unmeasured or unmeasurable operating conditions. However, most numerical schemes currently used for prediction purposes are based on steady-state schemes[4–6] and are unable to account for the highly unsteady phenomena occurring during rapid mixing. Some earlier attempts to include the effects of unsteady mixing[7] have resulted in somewhat improved predictions. In principle, simulation techniques such as large-eddy simulations could be used to understand and predict more accurately the unsteady mixing processes, but they are im-

Presented as Paper 92-0233 at the AIAA 30th Aerospace Sciences Meeting, Reno, NV, Jan. 6–9, 1992; received Jan. 27, 1992; revision received June 15, 1993; accepted for publication July 6, 1993. 

*Associate Professor, School of Aerospace Engineering. Member AIAA.
†Assistant Professor, Department of Mechanical Engineering.
‡Technical Staff, Combustion Research Facility.
§Assistant Professor, Department of Mechanical Engineering.

practical for engineering design analysis due to the substantial computational resources required. Therefore, there is a critical need to develop a more accurate yet simple model for unsteady mixing processes that can be used to model the unsteady processes occurring in the mixing region.

Accurate simulation of turbulent mixing and chemical reactions must take into account the physics of the mixing process. Studies of molecular mixing have shown that the mixing process generally consists of two steps: 1) the entrainment of the fluid from the two streams into the mixing region, and 2) the mixing of the fluids at the molecular level as they come into contact. Classical modeling of turbulent mixing in high Reynolds number flows typically assumes that turbulent convection dominates over molecular diffusion processes, i.e., the first step is the crucial one. However, experimental studies[8] have revealed that for flows at the same Reynolds number, both the mixing rates and the distribution of the mixed fluids are quite different in fluids of widely different molecular diffusivity. This clearly indicates that besides turbulent convection, molecular diffusion effects are important at the small scales. In terms of nondimensional parameters, this implies that the effects of both Reynolds number and Schmidt number on the mixing rate need to be taken into account. When chemical reactions are also occurring, then the Damkohler number effect will also need to be included.

Kerstein[9-11] took into account these results and developed a novel model called the linear-eddy model, which treats separately the effects of both turbulent mixing and molecular diffusion at the small scales. The motivation for these studies was to develop a configuration-invariant approach to study turbulent flows. Kerstein's results showed that a set of laws or models governing the processes of entrainment, turbulent mixing, and thermochemistry can be developed to provide a self-contained picture of the overall fluid mechanical and thermochemical structure of turbulent reacting flows. In the present study, this mixing model has been extended to include finite-rate kinetics, including NOx production, characteristics of realistic nonpremixed combustion in turbulent jet flames.

## II. Formulation of the Mixing Model

In this section, the various elements that constitute the stand-alone mixing model are identified and described. The stand-alone mixing model contains three major elements: 1) the basic unsteady mixing model that simulates the small-scale processes, 2) the application-specific processes that models the physical configuration, and 3) the finite-rate kinetics mechanism that models the combustion process in the small scale.

### A. Unsteady Mixing Model

The basic idea is to treat separately, two different mechanisms acting to describe the evolution of a scalar(s) (chemical species) in a specified domain. These two mechanisms are 1) molecular diffusion, and 2) turbulent convective transport. For flows in which finite-rate kinetics are occurring, an additional mechanism is incorporated, as discussed in Sec. II.C.

#### *1. Molecular Diffusion*

The first mechanism is molecular diffusion, which is implemented by the numerical time integration of the diffusion equation

$$\frac{\partial Y_k}{\partial t} = W_k + D_k \frac{\partial^2 Y_k}{\partial x^2} \tag{1}$$

where $Y_k$ is the $k$th species mass fraction, $W_k$ is the chemical production/destruction term for the $k$th species, and $D_k$ is the $k$th species diffusion coefficient. Note the absence of the convective term in this species diffusion equation. The turbulent convection is carried out separately by the second mechanism described in the next section. The strategy here is to resolve

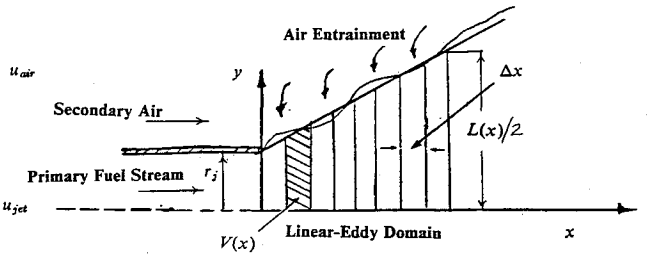


**Fig. 1 The geometry of the jet and the computational domain.**

all the relevant length scales involved in the local diffusion and transport processes. Since it is in the small scales where mixing and chemical reactions occur, resolution of the small scales is important. Therefore, to resolve all the small-scale processes taking part in the unsteady mixing, and to keep the computational cost reasonable, the domain is restricted to one dimension.

Consider the configuration shown in Fig. 1, which shows a fuel jet exiting into a mixing zone. This is a test geometry that corresponds to the mixing zone in the RQL combustor and to geometries in many jet flame experiments. If the streamwise $x$ direction is chosen as the linear-eddy domain, and if that domain is further subdivided into small cells, then each cell would represent a control volume, which is determined by the cell width $\Delta x$, and a radial zone extending from the centerline to the nominal jet radius $r_j$. The volume of each cell of width $\Delta x$ is then given by $V(x) = \pi r_j^2 \Delta x$. For the case shown in Fig. 1, the jet radius is given by the relation: $r_j(x) = C_s(x - x_0)$, where $x_0$ is the virtual origin and $C_s$ is an empirical constant which ranges from 0.07 in the forced-convection limit to 0.10 in the natural-convection limit.[11] The choice of $\Delta x$ is dependent on the smallest characteristic length scale (or eddy size) that needs to be resolved. We choose $\Delta x = L(x)/n$, where $L(x)$ is the integral length scale, which is given by $L(x) \approx 2r_j(x)$, and $n$ is the resolution factor, which is constant for a given computed realization. Using this definition of $L(x)$, the volume of each cell becomes $V(x) = (\pi/4)L(x)^2\Delta x$.

Since we are interested in the downstream evolution of the mixing region, the spatial evolution (spreading) of the jet needs to be incorporated. From experimental data, the spreading of the jet can be characterized by $L/d_\theta = (1 + c\bar{x})$, where $d_\theta$ is the momentum diameter of the jet, which is defined as $d_\theta = d_0\sqrt{\rho_0/\rho_a}$ with $d_0$ as the fuel jet nozzle diameter. Here, $\bar{x} = x/d_\theta$ is the nondimensional streamwise distance, and $c$ is a constant denoting the spatial spreading rate; typically, $c = 0.14$ for free jet. Also, $\rho_0$ and $\rho_a$ are, respectively, the density of the primary fuel stream at the fuel nozzle exit (i.e., at $x = 0$) and the ambient (air) density. Note that with this definition of $L(x)$, the cell width $\Delta x$ and the volume $V(x)$ increases in the downstream distance. The increase in the volume reflects the entrainment of air into the mixing region.

In addition to the specification of the spreading rate of the mixing layer, it is also necessary to decide the total streamwise extent of the mixing layer (the computational domain) that must be modeled. Experiments[12] suggest that a region of around $x/d_0 \approx 200$ needs to be modeled since the hydrogen flame length can be in the range of $x/d_0 = 100-140$. In the present calculations, the spatial extent of the mixing layer that was modeled exceeded $x/d_0 = 200$.

#### *2. Turbulent Convection*

The second mechanism in the mixing model is the turbulent convection process. This is incorporated in the model by a random process that rearranges the fluid element along the linear direction and is carried out (subject to some constraints) while the molecular diffusion process is going on. This process causes a random walk of the fluid elements and introduces a discontinuous (turbulent) fluid motion, representing small-scale turbulent stirring. Each event involves permutation of

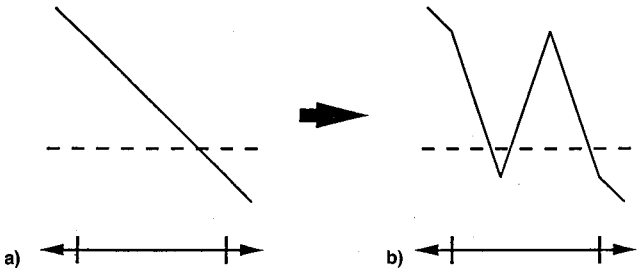


**Fig. 2 The effect of mapping on the scalar field: a) original scalar field before application of rearrangement and b) scalar field after rearrangement process. The scalar rearrangement (turbulent stirring) process carried out by the triplet map involves selecting a segment of the linear domain for rearrangement, making three compressed copies of the scalar field in that segment, replacing the original field by the three copies, and inverting the center copy.**

the cells of the spatially discretized concentration field and is confined to a finite segment of the total computational domain. This finite domain may be viewed as the size of the eddy that is causing the turbulent stirring. To bring the physics of turbulent transport into this process, the frequency of these events corresponding to a given range of eddy sizes is determined such that the principal scaling laws governing turbulent transport are satisfied.

To implement this process of turbulent transport, a mapping procedure called the triplet map was developed by Kerstein.[11] Figure 2 shows the effect of the triplet map in the continuum limit. Essentially, the size of the eddy, characterized by its length $l$ is first chosen from a probability distribution of eddy sizes $f(l)$. Then the scalar field (e.g., with a linear gradient as shown in Fig. 2a) within the chosen segment $l$ is compressed by a factor of 3, thus tripling the scalar gradient within the segment. The original scalar field within the segment $l$ is then replaced by three copies of this compressed field, with the middle copy reversed. The resulting scalar field is shown in Fig. 2b. This discrete mapping is defined so as to recover this rule in the continuum limit while satisfying species conservation exactly in the discrete implementation. More details of the theoretical considerations behind the triplet map are given by Kerstein.[10,11]

To carry out the triplet map, the size of the eddy $l$ must be first determined. The sizes of eddies present in the flow are assumed to range from the Kolmogorov microscale $\eta$ to the integral length scale $L$ (i.e., $\eta < l < L$), and the eddy size $l$ is chosen randomly from a power-law distribution $f(l)$ within this chosen range. Using Kolmogorov scaling, $Re_{l_0} \approx (l_0/\eta)^{3/4}$, Kerstein derived an expression for $f(l)$, which can be written as

$$f(l) = \frac{5}{3L} \frac{1}{(L/\eta)^{5/3} - 1} \left(\frac{l}{L}\right)^{-8/3} \tag{2}$$

Once the range of eddy sizes is known, a single inversion event involves first choosing an eddy size $l$ from the pdf $f(l)$ [Eq. (2)] and carrying out the mapping described above. Note that $f(l)$ varies with both $x$ and $t$. A sequence of such mappings must be carried out so that all allowable eddies within the chosen range take part in the process. The rate at which this mapping takes place is determined based on the local values, and therefore, varies both with time and with the spatial location in the mixing region. This rate is specified by a rate parameter $\lambda$, which has the unit of (length $\times$ time)$^{-1}$ and is determined by first determining the turbulent diffusivity of the random walk process for each eddy. Without going into detail (see Kerstein[9,10] the value of $\lambda$ can be determined as

$$\lambda = \frac{54}{5} \frac{\nu Re_L}{L^3} \frac{[(L/\eta)^{5/3} - 1]}{1 - (\eta/L)^{4/3}} \tag{3}$$

The time scale associated with the stirring events $\tau_s$ is related to $\lambda$ by the simple relation $\tau_s = 1/\lambda L$.

This completes the description of the basic model. To summarize, the unsteady mixing in a specified domain is modeled by two processes that work together but which are modeled separately. Molecular diffusion updates the concentration fields deterministically based on Fickian diffusion within a linear domain in which all the relevant small scales are resolved. Chemical heat release within each cell in the linear domain can also be included by solving the diffusion equations for $k$ species with the full chemistry model for $W_k$. However, the hydrogen-air, finite-rate kinetics are a multispecies mechanism with large production/destruction terms for $W_k$ (and, thus, small chemical times, $\tau_{ch}$). This can make the diffusion equation numerically stiff. Therefore, the finite-rate kinetics are implemented differently, as described in Sec. II.C.

While the molecular diffusion process is going on, it is punctuated by randomly occurring rearrangement events representing the turbulent convective stirring process. This stirring occurs at a frequency $\lambda$, as determined by the physical scaling laws described above, and results in the rearrangement of the species within each eddy of size $l$. Typically, the time (frequency) at which the mapping events take place ($\tau_s$) will be different than the time-step required for integrating the diffusion equation ($\tau_d$). This is taken into account in the algorithm.

### B. Application-Specific Processes

The basic processes, molecular diffusion, and turbulent mixing, must be further supplemented by application-specific processes that characterize the type of mixing process being studied. These application-specific processes are used to specify the boundary and the inflow/outflow conditions. By parametrically varying the important parameters of the application-specific process, the effect of different unsteady mixing strategies can be studied.

For the stand-alone model developed here, there are three application-specific processes that need to be modeled. These are 1) the fuel inflow, 2) the air entrainment, and 3) the streamwise motion and outflow of the jet. Each of these processes is described below.

#### 1. *Fuel Inflow*

Fuel enters the first cell of volume $V(0)$ at a constant mass flow rate $\dot{m}_0$ from the upstream state. The state conditions—e.g., the temperature, pressure, density, and the species mass fractions in the fuel mixture at the entrance to the mixing zone—need to be specified. In all the calculations described here, this state is specified. For the RQL combustor, this state may be the exit conditions from the primary zone.

#### 2. *Air Entrainment*

Air entrainment process is determined based on the length and time scales associated with the physical process. Thus, by proper modification of the entrainment law, the effect of different air injection strategies can be studied. Some preliminary study of modifying the entrainment process was carried out to identify the important time and length scales.[13]

From previous experimental observations of free jets, it is clear that the air will be entrained throughout the flow domain; however, it is not entrained in a continuous manner. Rather, air is entrained in finite parcels, and the size of the parcel directly influences the mixing process. From earlier experiments[14,15] it appears that the size of the parcel is comparable to the jet diameter. This information is included in the model by setting the volume of the entrained air parcel to be $V_E(x) = (\pi/4)L^3(x)$. Note that, since $L(x)$ is an increasing function with $x$, the volume of air entrained will also increase with streamwise distance. The frequency of the

entrainment events in the interval $(x, x + dx)$ is given by $\lambda_E(x)\,dx$, and is determined from the local entrainment rate

$$\frac{d\dot{m}_a}{dx} = \lambda_E(x)\rho_a V_E(x) \tag{4}$$

where $\dot{m}_a$ is the mass flux of the air crossing any $x$ plane and is obtained by using entrainment laws. Here we use an experimentally verified set of entrainment laws.[16] It was shown that the local entrainment rate can be modeled by[16]

$$\frac{d\dot{m}_a}{dx} = C_E\left(\frac{\pi\rho\dot{G}}{4}\right)^{1/2} \tag{5}$$

where $\rho = \dot{m}/\dot{V}$, and $\dot{V}$ and $\dot{G}$ are, respectively, the volume and momentum flux crossing any $x$ plane. Here, $C_E$ is an empirical coefficient that ranges from 0.32 in the forced-convection limit to 1.84 in the natural-convection limit.

The momentum flux $\dot{G}(x)$ is determined from the local momentum balance according to the relation

$$\frac{d\dot{G}}{dx} = \pi C_g g(\rho_a - \rho)b^2 \tag{6}$$

where $g$ is the gravitational acceleration, $C_g = 11.8$ is an empirical coefficient, and $b = r_j$ is the nominal jet radius defined earlier. Equation (5) is integrated with the inflow condition, $\dot{G}(0) = G_0$, where $G_0 = (\pi/4)\rho_0 u_0^2 d_0^2$, where subscript 0 denotes the fuel state at the inlet ($x = 0$). This result is combined with Eqs. (4) and (5) to obtain the entrainment rate $\lambda_E(x)$.

The entrainment events occurring at the frequency $\lambda_E$ are taken to be statistically independent (similar to the mapping events), and the process is implemented similar to the turbulent stirring process described earlier. Thus, the epochs and locations of the entrainment events are selected by an algorithm that parallels the stirring algorithm.

*3. Streamwise Motion*

When fuel enters the first cell, it must displace fluid in subsequent cells to maintain constancy of the cell volume. This displacement induces a streamwise flow. In some respects, this reactant-feed mechanism resembles earlier plug-flow studies (e.g., the coalescence-dispersion model).[17] However, there are two major differences. First, the radial spreading of the jet is included in the present model by virtue of the streamwise increase of the cell volumes (Fig. 1). Second, although the fuel enters at only one location the air is entrained throughout the streamwise direction, as shown in Fig. 1. Both these realistic mechanisms are included in the present model, whereas they are missing in the plug-flow mixing models.

Two other physical processes contribute to the streamwise motion: 1) the air entrainment process (described in Sec. II.B.2) and 2) the thermal expansion due to heat release. The effect of both these processes are similar to the effect of fuel inflow and induces a streamwise fluid displacement. Therefore, streamwise motion is a result of three processes. More details of the implementation of the streamwise motion are given elsewhere.[11,13]

### C. Finite-Rate Kinetics Within the Mixing Model

As noted above, conceptually, full finite-rate kinetics can be included within each cell of the computational domain during the molecular diffusion process. However, this can make the time-step very small and increase the overall computational cost. An approach that reduces the computational effort is to use reduced reaction mechanisms. This has been carried out using a hydrogen-air, nonpremixed jet flame as a test problem. More complex reduced mechanism for methane-air combustion will be studied in the future.

The hydrogen-air jet flame has been experimentally studied extensively.[12,18] Numerically, a reduced mechanism model was recently used with a pdf method to predict the flow properties.[19,20] The primary advantage of using the reduced mechanism approach is the reduction in the number of scalar equations that must be solved. For the hydrogen-air problem, only two scalars—the mixture fraction $\xi$ and a progress variable $n$—need to be solved to obtain all other properties. Also, the reaction mechanism can be solved first to generate a "look-up" table that can then be used to interpolate for the species information whenever required. This clearly reduces the amount of computation required.

In the hydrogen-air, nonpremixed jet flame considered here, the total number of scalars is 10, which are the seven active chemical species (i.e., $H_2$, $O_2$, $H_2O$, O, H, OH, $HO_2$), plus temperature, pressure, and density. If we assume equal diffusivities for species and enthalpy, the mixing process can be described by a conserved scalar $\xi$. The mixture fraction is defined as the normalized mass fraction of an atomic species originating in the fuel stream. With this definition, the concentrations of atomic species are linearly related to $\xi$.

A partial equilibrium model approach is used here,[19] which assumes that some of the reactions are relatively fast compared to the three-body recombination steps. The total number of moles per unit mass $n$ is chosen as the reactive scalar, which is given as

$$n = n_{H_2} + n_{O_2} + n_{H_2O} + n_O + n_H + n_{OH} + n_{HO_2} + n_{N_2} \tag{7}$$

The details of the reduced mechanism has been described extensively,[19] and therefore, it will not be described here. Two types of hydrogen-air combustion process have been studied: 1) a pure hydrogen-air case and 2) a 22% argon + 78% hydrogen-air case.

The NO production mechanism in the $H_2$-air flame modeled here is primarily from the thermal pathways. Thus, for now, the prompt NO formation and the formation of NO involving intermediate $N_2O$ are neglected. This is considered acceptable, since, in general, the majority of NO formed in hydrogen-air combustion is from the thermal NOx pathways. The thermal NO reactions are described by the well-known Zeldovich mechanism, and a steady-state assumption for the N atom and $(NO)/(NO)_{equil} \ll 1$ are assumed. This results in a reduced Zeldovich mechanism: $N_2 + O_2 = 2NO$ and the NO formation rate (gm/cm$^3$-s) can be approximated as[20]

$$S_{NO} \approx 2k_{f,nr1}(N_2)(O)M_{NO} \tag{8}$$

where $(C)$ denotes the concentration of species $C$ (mole/cm$^3$), $M_{NO}$ is the molecular weight of NO, and $k_{f,nr1} = 1.84 \times 10^{14}\exp(-38370/T)$ cm$^3$/mole-s.

The diffusion problem analogous to Eq. (1) for this hydrogen-air case is the solution of three equations for the mixture fraction $\xi$, the progress variable $n$, and the NO moles $n_{NO}$:

$$\frac{\partial\xi}{\partial t} = D_\xi\frac{\partial^2\xi}{\partial x^2} \tag{9}$$

$$\frac{\partial n}{\partial t} = D_n\frac{\partial^2 n}{\partial x^2} + \left(\frac{dn}{dt}\right)_\xi \tag{10}$$

$$\frac{\partial n_{NO}}{\partial t} = D_{n_{NO}}\frac{\partial^2 n_{NO}}{\partial x^2} + \left(\frac{dn_{NO}}{dt}\right) \tag{11}$$

Here, the source term in Eq. (10) is obtained from the look-up table for the reduced mechanism, and the NO production term is determined from Eq. (8). Also, for this study, we assumed that $D_\xi = D_n + D_{n_{NO}} = \nu/Sc$, where $\nu(T)$ is determined using the Sutherland's law, and $Sc$ is the Schmidt number taken to be unity.

## III. Implementation of the Stand-Alone Mixing and Reaction Algorithms

The implementation of the mixing and reaction algorithms as a stand-alone model is relatively straightforward. The elements of the model described in Sec. II involves six separate mechanisms: 1) the fuel feed into the mixing zone; 2) the air entrainment throughout the mixing zone; 3) the molecular diffusion; 4) the turbulent stirring and 5) the finite-rate kinetics within each cell; and 6) the streamwise motion resulting from the effects of fuel feed, air entrainment, and thermal expansion due to combustion. The implementation of these mechanisms is outlined below.

First, molecular diffusion and chemical kinetics are simulated by time integration of the diffusion Eqs. (9–11) within the computational domain using a standard finite-difference (central difference) approach. Typically, the time-step for the numerical integration is $\tau_d = C\Delta x_{\min}^2/D$, where $\Delta x_{\min}$ is the size of the smallest cell and $C < 0.5$ for stability.

The other main mechanism, i.e., the rearrangement events that models small-scale turbulent stirring, is also carried out whenever the epoch for the mapping event is reached during the time integration of the diffusion equations. Typically, the epoch of the mapping event is randomly selected based on the overall rate, $R = \lambda L$, of such events. When this time is reached, the location of the eddy is selected with uniform likelihood within the cell, and an eddy size is chosen by randomly sampling the pdf $f(l)$. Then the mapping process is carried out as described earlier. This exchange is assumed to occur simultaneously and instantaneously so that no time elapses during this process. After this event, the epoch of the next event is determined based on the new value of the event rate $R$.

Similar to the turbulent stirring events, the entrainment of the air parcels into each cell is determined based on the entrainment laws and the entrainment frequency $\lambda_E$; also, the epochs and locations of the entrainment events parallel the previously described turbulent stirring process.

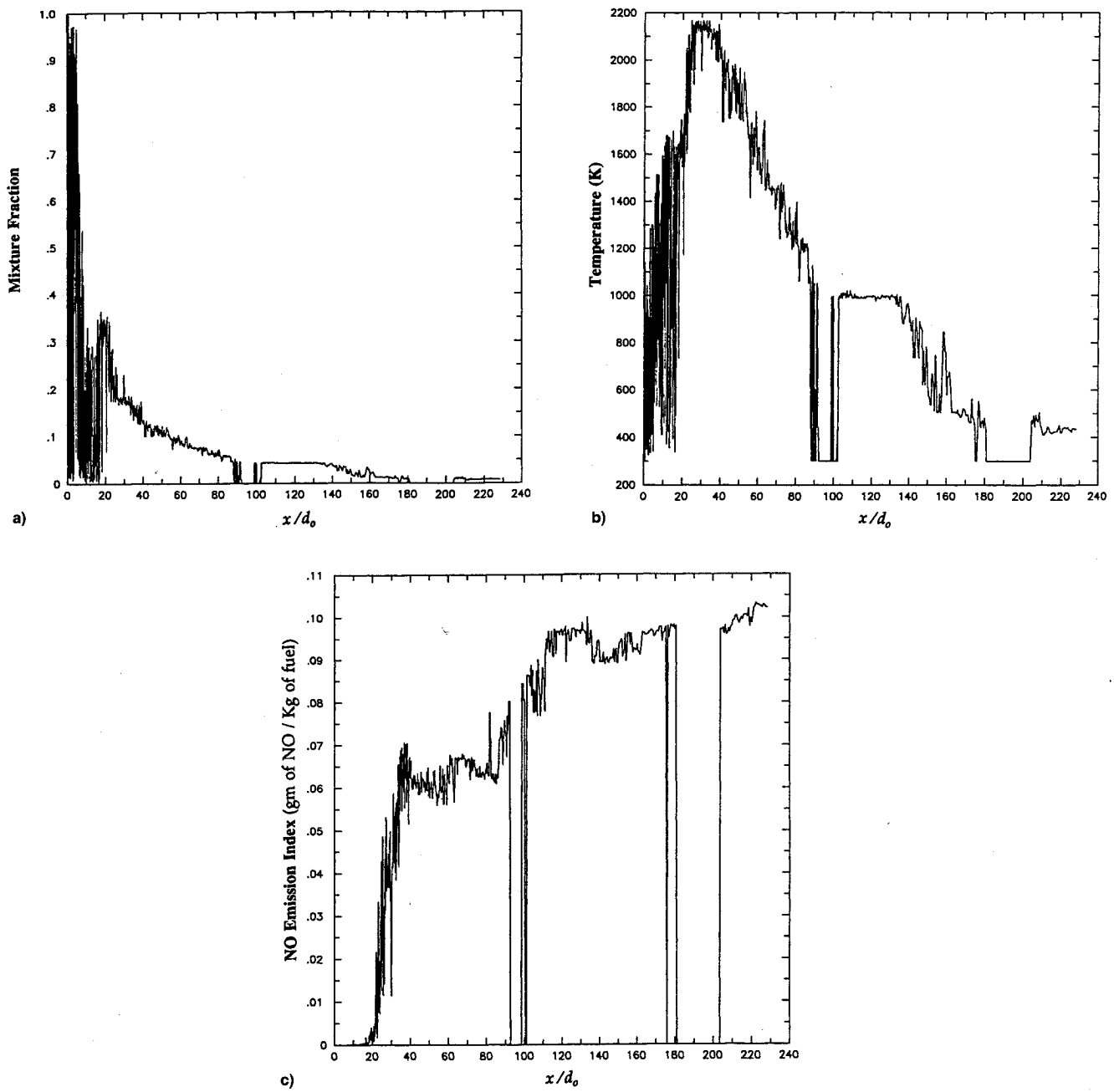


**Fig. 3. Instantaneous axial variation of the flow properties in the jet flame for a jet speed of 222 m/s and a jet diameter of 0.52 cm: a) mixture fraction ($\xi$) as a function of axial location, b) temperature (K) as a function of axial location, and c) NO emission index as a function of axial location.**

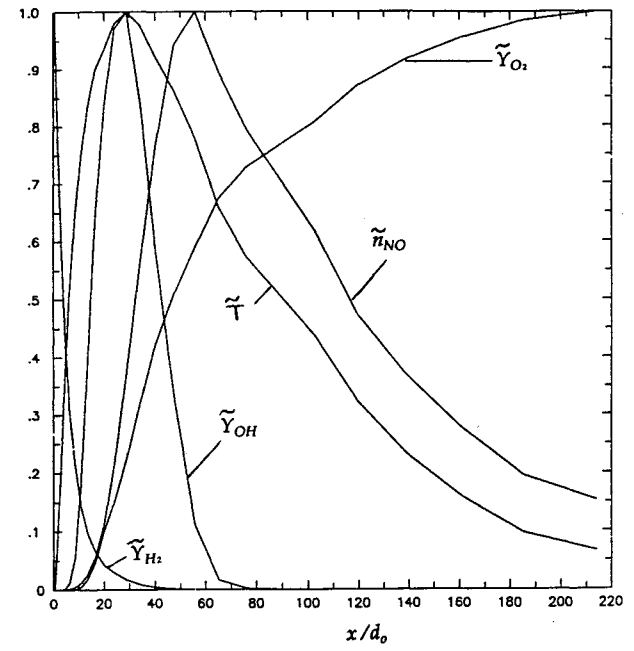


**Fig. 4 Axial variation of the mean flow properties for a jet speed of 225 m/s and a jet diameter of 0.52 cm. All variables have been normalized by their maximum value.**

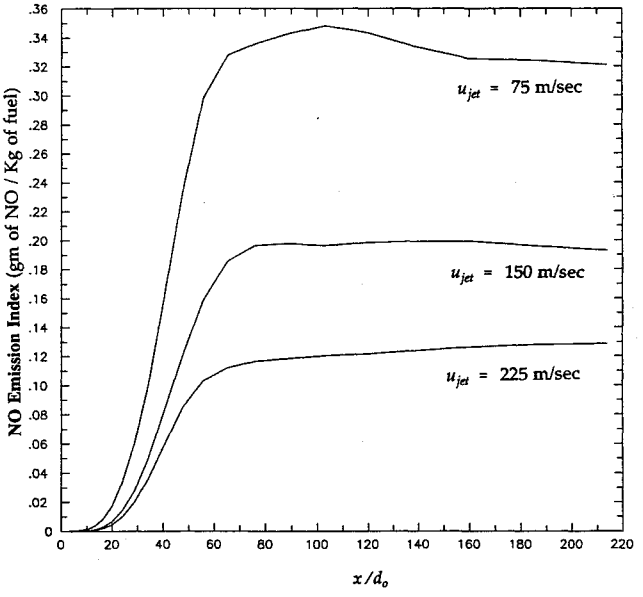


**Fig. 5 Axial variation of the NO emission index for various jet speeds.**

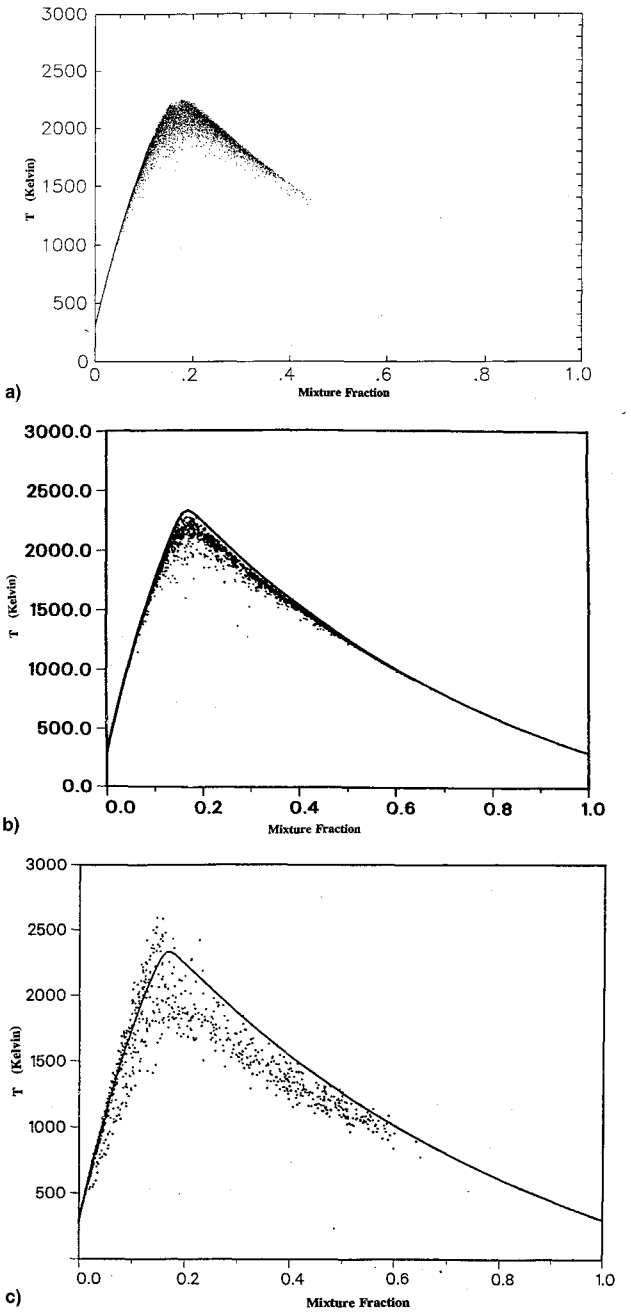


**Fig. 6 Scatter plot of temperature vs mixture fraction at $x/d_0$ = 30 for a fuel jet speed of 150 m/s: a) present calculations, b) pdf calculations,[19] and c) experimental results.[18]**

The fuel feed, air entrainment, and thermal expansion due to combustion, all induce streamwise fluid displacement, which represents the streamwise flow. This displacement process is implemented as a distinct computational step that incorporates all three contributions. After the fuel feed, air entrainment, and combustion during a time-step have been completed, the deviation of the cell densities from their equilibrium values is used to determine new equilibrium values using perfect gas law and a streamwise adjustment (which essentially incorporates the downstream flow motion) of the fluid properties in the cells carried out to adjust the properties in each cell. More details of the implementation of the streamwise motion are given by Kerstein.[11]

## IV. Results and Discussion

For the hydrogen-air problem, the initial values of $\xi$ and $n$ in the fuel jet are specified depending upon the type of fuel used and the ambient conditions. The fuel jet enters the mixing domain with $\xi = 1$ and $n = 0.496$ (for the 22% Ar + 78% hydrogen case, $n = 0.0965$), and with a temperature of 300 K. The entrained air is at a state given by $\xi = 0$ and $n = 0.03466$, and a temperature of 300 K. The combustion process is assumed to occur at the standard atmospheric pressure condition. The stoichiometric conditions for the $H_2$-air flame are: $\xi_{st} = 0.028$ and $n_{st} = 0.0412$, with a flame temperature of 2193 K, while for the 22% Ar + 78% $H_2$-air flame the stoichiometric conditions are: $\xi_{st} = 0.1636$ and $n_{st} = 0.0388$, with a flame temperature of 2303 K.

During the computations, the spatial distribution of the scalar fields will continuously evolve, and eventually the flow will reach a statistically steady state. The instantaneous realizations obtained over a long period of simulation were then Favre-averaged to obtain the statistically steady-state flowfield. To obtain the steady-state field, the total number of grid points (1250 in the present case) is divided into blocks each containing 50 cells; each block is then further divided into bins containing 10 cells each. Favre-averaging of the flow

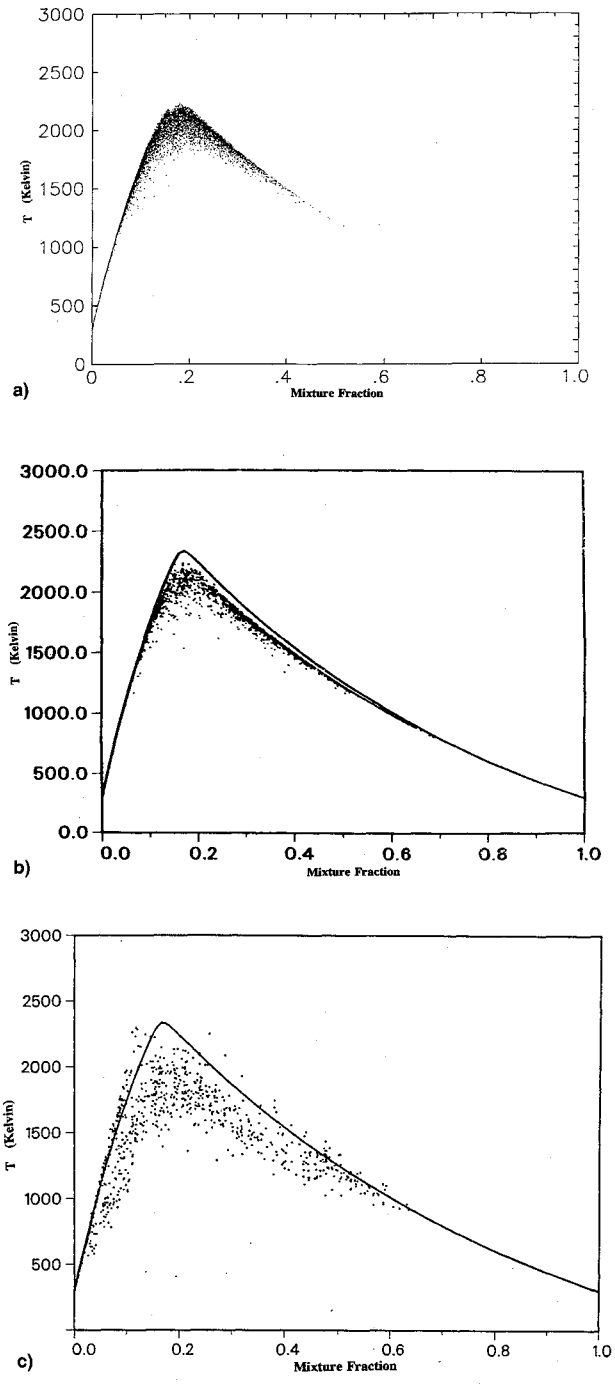


**Fig. 7 Scatter plot of temperature vs mixture fraction at $x/d_0 = 30$ for a fuel jet speed of 225 m/s: a) present calculations, b) pdf calculations,[19] and c) experimental results.[18]**

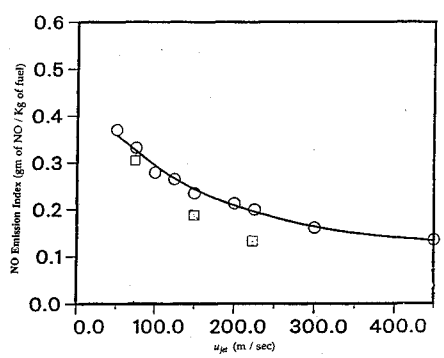


**Fig. 8 Variation of the NO emission index as a function of jet speed. Circles and curve fit: pdf results,[20] square: present results.**

variables is then carried out over each bin (10 cells) to obtain the averaged property. The effect of grid resolution on the accuracy of the data was also addressed by repeating some of the calculations with twice the above noted resolution. It was determined that for the conditions studied here, a resolution of 1250 cells was sufficient. Most of the results presented here are in terms of these Favre-averaged properties, since these are typically the properties required for design and prediction.

Although simulations for a variety of flow conditions and fuel types were carried out, here we will concentrate on the results obtained for the 22% argon-hydrogen jet flame case. Figures 3a–3c show an instantaneous realization of the flow properties in the jet flow. Figure 3a shows the axial variation of the mixture fraction $\xi$ for a fuel jet speed of 225 m/s. Figure 3b shows the temperature variation in the jet and Fig. 3c shows the axial variation of the instantaneous NO emission index (defined as gm of NO/kg of fuel) for the same case. These profiles show the characteristic fluctuations due to the turbulent mixing process modeled by the linear-eddy mapping procedure. Figure 3a shows that the mixture fraction decreases from the fuel jet inflow conditions at $x/d_0 = 0$ to very low values in the far field, while the temperature field shows a distinct peak at around $x/d_0 = 40$. At around the same axial location, the NO emission index (NOEI) (Fig. 3c) increases rapidly from negligible value to a large value that eventually levels off in the far field. The axial variation of NOEI observed here is similar to that observed in the experiments.

The Favre-averaged, steady-state results also show similar results. Figure 4 shows the time-averaged properties computed for the same case as in Fig. 3. The mean temperature, the mean species fraction for $H_2$, $O_2$, OH, and the mean NO moles per unit mass are plotted (normalized by their maximum value) in the same figure to facilitate comparison. It can be seen that the fuel (hydrogen) mass fraction decreases rapidly in the downstream direction, while the oxygen mass fraction increases downstream due to air entrainment. The hydroxyl radical peaks at the same location of the peak temperature (at around $x/d_0 = 40$); however, it is interesting to note that the maximum value of NO occurs further downstream (at around $x/d_0 = 70$) of the peak temperature location.

Figure 5 compares the axial variation of the NO emission index for three jet speeds. These results clearly show that the NO emission index increases rapidly near where peak temperature occurs and then asymptotically levels off at a value that is typically considered the NOEI of the jet. It can be seen that as the jet speed increases, the NOEI decreases. This trend of decrease in the emission index with increase in jet speed agrees with experimental observation.[12]

Figures 6a–6c show, respectively, the present computations, the experimental data,[18] and the earlier pdf computations[19] in terms of the $T$-$\xi$ scatter at $x/d_0 = 30$ for the fuel jet speed of 150 m/s. Figures 7a–7c show, respectively, these three plots for the jet speeds of 225 m/s. Clearly, the present computations are capable of reproducing quite accurately the experimental and pdf predictions. Both the magnitude of the peak temperature and its location (as a function of $\xi$) agrees with both the experimental and pdf data. The solid line in the experimental and the pdf calculations shows the equilibrium temperature-mixture fraction relation. As expected, all the computed results fall below this line and clearly show the effect of finite rate kinetics. The scatter in the experimental data above the adiabatic temperature is due to the noise in the measurement.

Finally, Fig. 8 shows the variation of the NO emission index as a function of fuel jet speed for a given jet diameter. Also shown in this figure is the pdf predictions.[20] The present prediction also shows the same trend, i.e., the NO emission index decreases with increasing jet velocity for the same fuel jet diameter. This result is again consistent with past observations and is consistent with the notion that as the jet speed increases, the characteristic residence time in the jet decreases,

resulting in lower NO production. The trend predicted by the present calculations is in good agreement with the pdf calculations. Direct comparison shows that there are differences in the value of NOEI predicted by these two methods. This could be attributed to the differences in the modeled configurations. For example, the pdf computations employed a surrounding coflowing air at a velocity of around 9.2 m/s (the present study assumes that there is no coflowing air). Also, the specific geometry used in the experiments (coaxial tubes with a pilot flame) was different from the geometry modeled in the present study. Regardless of these differences, the present one-dimensional model simulations demonstrate a capability to predict important features such as the NO emission of a jet flame. Since the method is quite general, other types of reacting jets, such as a methane-air and propane-air jet flows can be easily investigated by incorporating proper reduced mechanisms.

## V. Conclusions

In this article, a new mixing model is described that takes into account the fundamental features of turbulent mixing. Both turbulent mixing and molecular diffusion in the small scales have been identified in experiments to be important in flows with chemical species. By specifically separating these two effects and modeling them in the small scales, the mixing model developed here has a capability that all previous mixing models have lacked. This mixing model was used to study hydrogen-air, nonpremixed flame combustion using a reduced reaction mechanism, and the NO production in such flames due to the thermal mechanism (the Zeldovich mechanism) was also calculated.

The results show that finite-rate kinetics in the form of a reduced mechanism can be easily incorporated within the framework of the mixing model. Comparison of the present results with experimental data clearly demonstrate the strength of the stand-alone mixing model. This mixing model can be utilized to carry out parametric study to understand the importance of the various parameters that govern the mixing between fuel and entrained air. For example, the method of air entrainment can be modified to simulate different mixing strategies. The effect of different operating regimes, such as, high pressure on the NO production can be determined by using different look-up tables (which can be easily generated). Such studies may be able to identify the critical parameters that govern the NO production in mixing regions characteristic of the RQL quench zone. Once such parameters are identified, they can be parametrically varied to determine their effect on the NO production. There may exist certain ranges of these parameters where NO production is minimized. This information could be utilized to design physical mixing methods that could then be evaluated experimentally to determine its applicability to the RQL combustor. A point to be noted here is that the present approach is computationally very efficient (all simulations can be easily performed on desktop PCs or workstations in a matter of a few hours); thus, parametric studies can be carried out economically.

Another potential application of this mixing model is its use within steady-state codes so that the steady-state predictions take into account the unsteady small-scale processes that govern scalar mixing and combustion. Recently, a modified version of the present model was implemented as a subgrid model to study turbulent premixed combustion[21] and turbulent diffusion flames.[22] In this approach, the mixing model described in this article (with some minor modifications) is implemented within each of the computational grid cells. A similar approach is currently being studied for implementation in steady-state codes.

## Acknowledgments

This work was supported in part by NASA Lewis Research Center under Contract NAS3-26242, while the first author was at Quest Integrated, Inc., the Division of Engineering and Geosciences, Office of Basic Energy Sciences, U.S. Department of Energy, and the Advanced Combustion Engineering Research Center, University of Utah.

## References

[1]Bahr, D. W., "Gas Turbine Engine Emission Abatement—Status and Needed Advancements," *Gas Turbine Combustor Design Problems*, edited by A. H. Lefebvre, Hemisphere, New York, 1980.

[2]Tacina, R. R., "Low NOx Potential of Gas Turbine Engines," AIAA Paper 90-0550, Jan. 1990.

[3]Ott, J., "Researchers Seek Technologies for Quiet, Environmentally Safe SST," *Aviation Week and Space Technology*, June 18, 1990, pp. 94–98.

[4]Correa, S. M., and Shyy, W., "Computational Models and Methods for Continuous Gaseous Turbulent Combustion," *Progress Energy Combustion Science*, Vol. 13, 1987, pp. 249–292.

[5]Nguyen, L. H., and Bittker, D. A., "Investigation of Low NOx Staged Combustor Concept in High-Speed Civil Transport Engines," NASA TM 101977, July 1989.

[6]Rizk, N. K., and Mongia, H. C., "Three Dimensional NOx Modeling for Rich/Lean Combustion," AIAA Paper 93-0251, Jan. 1993.

[7]Pope, S. B., and Correa, S. M., "Joint PDF Calculations of a Non-Equilibrium Turbulent Diffusion Flame," *21st Symposium (International) on Combustion*, The Combustion Institute, Pittsburgh, PA, 1986, pp. 1341–1348.

[8]Dimotakis, P. E., "Turbulent Free Shear Layer Mixing," AIAA Paper 89-0262, Jan. 1989.

[9]Kerstein, A. R., "Linear-Eddy Model of Turbulent Scalar Transport and Mixing," *Combustion Science and Technology*, Vol. 60, Nos. 4–6, 1989, pp. 391–421.

[10]Kerstein, A. R., "Linear-Eddy Modeling of Turbulent Transport II: Application to Shear Layer Mixing," *Combustion and Flame*, Vol. 75, Nos. 3–4, 1989, pp. 397–413.

[11]Kerstein, A. R., "Linear-Eddy Modeling of Turbulent Transport. Part 4: Diffusion-Flame Structure," *Combustion Science and Technology*, Vol. 81, Nos. 1–3, 1992, pp. 75–96.

[12]Chen, H.-H., and Driscoll, J. F., "Nitric Oxide Levels of Jet Diffusion Flames: Effects of Coaxial Air and Other Mixing Parameters," *23rd Symposium (International) on Combustion*, The Combustion Institute, Pittsburgh, PA, 1990, pp. 281–288.

[13]Menon, S., "A New Unsteady Mixing Model to Predict NO Production During Rapid Mixing in a Dual Stage Combustor," AIAA Paper 92-0233, Jan. 1992.

[14]Dahm, W. J. A., and Dimotakis, P. E., "Measurements of Entrainment and Mixing in Turbulent Jets," *AIAA Journal*, Vol. 25, No. 9, 1987, pp. 1216–1223.

[15]Mungal, M. G., and Hollingsworth, D. K., "Organized Motion in a Very High Reynolds Number Jet," *Physics Fluids A*, Vol. 1, No. 10, 1989, pp. 1615–1623.

[16]Becker, H. A., and Yamazaki, S., "Entrainment, Momentum Flux and Temperature in Vertical Free Turbulent Diffusion Flames," *Combustion and Flame*, Vol. 33, No. 2, 1978, pp. 123–149.

[17]Butler, G. W., and Pratt, D. T., "Coalescence/Dispersion Modeling of Turbulent Combustion in a Jet-Stirred Reactor," *AIAA Journal*, Vol. 24, No. 11, 1986, pp. 1817–1822.

[18]Magre, P., and Dibble, R. W., "Finite Rate Kinetic Effects in a Subsonic Turbulent Hydrogen Flame," *Combustion and Flame*, Vol. 73, No. 2, 1988, pp. 195–206.

[19]Chen, J.-Y., and Kollmann, W., "Chemical Models for Pdf Modeling of Hydrogen-Air Nonpremixed Turbulent Flames," *Combustion and Flame*, Vol. 79, No. 1, 1990, pp. 75–99.

[20]Chen, J.-Y., and Kollmann, W., "Pdf Modeling and Analysis of Thermal NO Formation in Turbulent Nonpremixed Hydrogen-Air Jet Flames," *Combustion and Flame*, Vol. 88, Nos. 3–4, 1992, pp. 397–412.

[21]Menon, S., McMurtry, P. A., and Kerstein, A. R., "A Linear Eddy Mixing Model for LES of Turbulent Combustion," *Large-Eddy Simulations of Complex Engineering and Geophysical Flows*, edited by B. Galperin and S. A. Orszag, Cambridge University Press, New York, 1993.

[22]McMurtry, P. A., Menon, S., and Kerstein, A. R., "A New Subgrid Model for Turbulent Combustion: Application to Hydrogen-Air Combustion," *23rd Symposium (International) on Combustion*, The Combustion Institute, Pittsburgh, PA, 1993, pp. 271–278.